International Journal of Extreme Manufacturing

Enhanced ablation efficiency for silicon by femtosecond laser microprocessing with GHz bursts in MHz bursts(BiBurst)

OPEN ACCESS
IOP Publishing | IMMT
International Journal of Extreme Manufacturing
Int. J. Extrem. Manuf. 4 (2022) 015103 (9pp)
https://doi.org/10.1088/2631-7990/ac466e

Enhanced ablation efficiency for silicon by femtosecond laser microprocessing with GHz bursts in MHz bursts(BiBurst)

Francesc Caballero-Lucas, Kotaro Obata and Koji Sugioka*

RIKEN Center for Advanced Photonics, 2-1 Hirosawa, Wako-shi, Saitama 351-0198, Japan

E-mail: ksugioka@riken.jp

Received 3 September 2021, revised 19 October 2021
Accepted for publication 26 December 2021
Published 20 January 2022

Abstract

Ultrashort laser pulses confine material processing to the laser-irradiated area by suppressing heat diffusion, resulting in precise ablation in diverse materials. However, challenges occur when high speed material removal and higher ablation efficiencies are required. Ultrafast burst mode laser ablation has been proposed as a successful method to overcome these limitations. Following this approach, we studied the influence of combining GHz bursts in MHz bursts, known as BiBurst mode, on ablation efficiency of silicon. BiBurst mode used in this study consists of multiple bursts happening at a repetition rate of 64 MHz, each of which contains multiple pulses with a repetition rate of 5 GHz. The obtained results show differences between BiBurst mode and conventional single pulse mode laser ablation, with a remarkable increase in ablation efficiency for the BiBurst mode, which under optimal conditions can ablate a volume 4.5 times larger than the single pulse mode ablation while delivering the same total energy in the process.

Keywords: BiBurst mode, GHz burst, laser ablation, surface microfabrication

1. Introduction

Femtosecond laser pulses are being employed in an increasing number of applications for materials processing owing to their excellent performance that other conventional lasers cannot achieve [1–7]. Specifically, the ultrashort pulse duration of femtosecond lasers intensely confines the delivery of laser pulse energy in a duration shorter than the common time scales for transferring absorbed laser energy to the irradiated material lattice [8]. Consequently, the interaction between laser pulses and the processed materials becomes restricted to the irradiated area, ensuring a higher fabrication precision and better finishing quality of the processed areas, both are due to the notable suppression of the formation of the heat affected zone in the volume surrounding the irradiated spots [9]. Thus, laser ablation with femtosecond laser pulses achieves high microfabrication performance in terms of precision and quality. But, the industrial use of femtosecond laser processing should improve the overall throughput of the microfabrication process so as to be comparable or even superior to other microfabrication techniques.

A first approach to solve this would be increasing the power of the laser systems delivering the laser pulses for irradiation. Higher power can be achieved by either increasing the pulse energy or repetition rate. However, the former case produces higher intensities, which suffer from plasma shielding and collateral thermal damage, which compromises the benefits of femtosecond laser pulse microprocessing [10]. Multibeam parallel processing with higher power laser is a good solution to increase throughput [11–13], but it is another aspect that differs from the main scope of this paper. The latter case

* Author to whom any correspondence should be addressed.

2631-7990/22/015103+9$33.00

also induces thermal influence due to the diffusion of accumulated heat [14], resulting in the deterioration of microfabrication quality.

As an alternative, the use of bursts of ultrafast pulses has been proposed to improve ablation efficiency with better ablation quality. In this approach, the interaction between the laser pulses and the processed material takes place in a short total duration for the irradiation process. The total irradiation time in burst mode ultrafast laser ablation is so short that heat transfer to the material remains greatly restricted to the irradiated area, with very low diffusion to the surrounding material because most of the accumulated heat is carried away by the ablated material, known as ablation cooling [15]. Under these circumstances, the material gets heated and melts in a more controlled manner, which leads to higher efficiency and higher finishing quality for the microfabrication process.

Multiple experiments carried out by different research groups have shown the benefits and limitations of implementing ultrafast laser pulses in GHz burst mode mostly in metals like copper, stainless steel, and aluminum [16–20], as well as some preliminary results in silicon [16, 17, 21]. Until now, the cited experiments have focused on processing metals mostly via milling or analysis limited to the use of GHz burst mode.

In this paper, we extend these studies to apply GHz bursts in MHz bursts, known as BiBurst mode, on a well-known and widely used semiconductor, silicon. Until now, BiBurst mode has been explored only in metals [18, 19]. The obtained results are compared with conventional ablation using single pulse train (single pulse mode) and a single GHz burst pulse. Detailed analysis is carried out to investigate the efficiency of the ablation process for the various tested experimental conditions to show the ability of BiBurst for ablating larger volumes of Si with higher efficiency, unlike metals, and to propose a possible mechanism.

2. Experimental

The results presented in this paper were obtained by treating a *p*-doped crystalline silicon wafer with 625 μm thickness, crystalline orientation (100), and conductivity of 3.11–3.41 Ω cm with an experimental setup developed for laser ablation studies. The main element of the experimental setup was the femtosecond laser system with BiBurst mode capability. The laser system (Pharos, Light Conversion) delivered femtosecond laser pulses with a pulse duration of 220 fs at a near-infrared wavelength of 1030 nm. Yb active medium generated the laser pulses. Thanks to the pulse picking capabilities of the system, the laser pulses were provided at tunable repetition rates up to 1 MHz, reaching a maximum output power of 10 W.

Laser pulses supplied by the femtosecond laser system propagated through some elements in the experimental setup, shown in figure 1, until reaching the material sample to be processed. Right before, the original 2.5 mm diameter Gaussian laser beam was focused through an objective lens

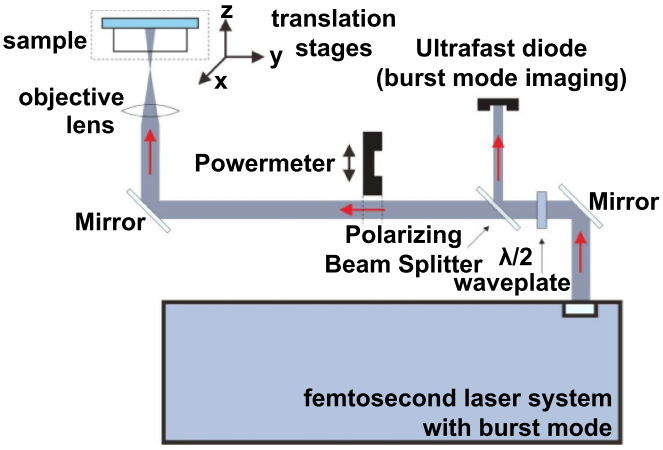

Figure 1. Schematic of the experimental setup used for the burst mode ultrafast laser ablation.

with a numerical aperture of 0.4 onto the sample surface with a spot size of 1.9 μm in diameter at the beam waist. To ensure the optimal focusing condition of the laser beam on the sample surface with the smallest possible beam spot size, an autofocus system was used coaxially to the incident laser beam.

A part of the beam was reflected at a beam splitter and directed along the laser path to an ultrafast photodiode connected to an oscilloscope for imaging the temporal profile of the laser pulses grouped in bursts.

As described above, BiBurst mode combines bursts of pulses at a GHz repetition rate inside a bigger packet of pulses at a MHz repetition rate. For this, we use the letter P to designate the number of pulses in a GHz burst (intrapulse number) and N for the number of bursts at the MHz repetition rate (burst number). The total group of N bursts, each containing P intrapulses, is referred to as the pulse packet.

For a proper comparison of the different burst mode configurations, experiments were carried out by delivering the same total packet energy (same total laser power) for each series. This means that the total energy E fixed for any BiBurst condition is evenly distributed into the total number of pulses $N \times P$ (product of the P intrapulses in a GHz-burst by the N MHz-bursts). Hence, the average energy for each intrapulse in the burst is $E/(N \times P)$.

Figure 2 shows the temporal distributions of the laser pulse energy for two different configurations of BiBurst modes and a single laser pulse (black line), which correspond to the voltages detected at the ultrafast photodiode. The single laser pulse has the highest intensity peak because all the energy is concentrated in it. The blue line, corresponding to two bursts ($N = 2$) containing two intrapulses ($P = 2$) each, reaches a lower peak intensity since the total laser power is kept constant for these configurations. The red line shows five bursts ($N = 5$, only two appear in the main plot because of the long time separation, while the whole pulse packet can be seen in the inset) containing two intrapulses ($N = 2$) each with further

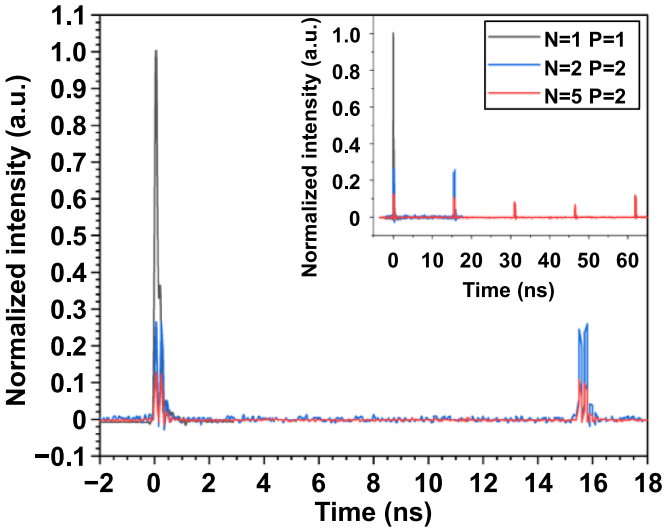

Figure 2. Normalized intensity reached by each laser pulse in the bursts for a selection of a different number of pulses in a GHz burst P (1 and 2) and a number of MHz bursts N (1, 2, and 5) explored in the experiments. As can be observed, the two BiBurst mode conditions (blue and red lines) and the single pulse (black line) carry the same total energy. The inlet exhibits a longer time domain to show all pulses for $N = 5$.

lower peak intensity due to a total pulse number of 10. In this figure, it can be seen how pulses with peaks that follow an almost flat tendency are grouped in bursts. The time separation between succeeding pulses in a GHz burst (intrapulse repetition rate) was measured at 205 ps, giving the ultrafast intra-pulse repetition rate of 4.88 GHz. The laser system provided GHz bursts ranging from 1 pulse (single pulse mode) up to 25 pulses. The time separation between GHz bursts was 15.6 ns, corresponding to the interburst repetition rate of 64.1 MHz.

Additionally, a power meter temporarily intercepting the laser beam was used to monitor the incident laser power on the sample. The power could be adjusted by combining a polarizing beam splitter and a half-wave plate mounted on a motorized rotating stage.

By using this system, experiments were performed in the following way: the pristine silicon sample was irradiated with one BiBurst condition per irradiated spot, and multiple spots were prepared at different conditions on the same sample. For that, the sample was placed on a three-axis stage system that made it possible to control the sample position where the laser pulses impinged. A series of spots was ablated at different powers in a fixed burst mode configuration, and multiple BiBurst mode configurations were explored.

For the characterization and measurement of the ablated spots, scanning electron microscopy (SEM) observation and laser scanning microscopy (LSM) measurements were performed to study the morphology and dimensions of the processed spots. Based on the obtained results, ablation efficiency was evaluated and compared for GHz burst mode, BiBurst mode, and single pulse mode conditions delivering the same total power.

3. Results and discussion

Laser ablation experiments performed according to the procedures described above formed craters at the surface of the processed silicon sample. A series of craters obtained by bursts of pulses delivering the same total packet energy of 0.53 μJ but under different conditions of the temporal distributions of the energy can be observed in figure 3.

A first observation of the SEM images gives evidence of the different morphology and dimensions of the craters at the irradiated spots for the various burst mode configurations. In all of them, material melting in the irradiated area and a partial redeposition of the melted material surrounding the ablated area defined by the central circular contour were detected, even at the ultrashort duration of single pulse irradiation. In this case, corresponding to figure 3(a), the concentration of all of the energy in a single pulse resulted in a high peak laser intensity that produced a crater with an evident rim surrounding it accompanied by multiple droplets of the redeposited material ejected during the ablation process. The presence of redeposited material was reduced in the case of GHz burst mode ablation with one burst containing 25 intrapulses ($N = 1$, $P = 25$) (figure 3(b)) and for the BiBurst mode condition of two bursts containing 25 intrapulses per burst ($N = 2$, $P = 25$) (figure 3(c)), resulting in a sharper contour of the ablated crater, with better defined and more abrupt boundaries between the ablated area and the surrounding pristine material. However, ablated material redeposition clearly increased for larger numbers of bursts (BiBurst condition of $N = 5$ and $P = 25$) (figure 3(d)). This suggests that the successive energy deposition inducing gentle heating with GHz burst mode ablation in silicon [21] is beneficial for the ablation process, achieving better ablation surface quality when there are not too many bursts, which is the case of $N = 2$ and $P = 25$. In comparison, the larger number of bursts ($N = 5$, $P = 25$) seems to still benefit from the ultrafast material heating but increases the amount of redeposited material, indicating a larger detrimental effect of the material heating. Another relevant tendency that can be observed in figure 3 is the reduction of the ablated area with increasing N and P.

To gain more information about the morphology and dimensions of the ablated spots, the cross-sectional profiles of the same craters shown in figure 3 were measured by LSM, as shown in figure 4. A first clear result is that BiBurst mode ablation forms deeper craters. For GHz burst mode conditions (red line corresponding to $N = 1$ and $P = 25$), the ablated crater is deeper than that obtained by single pulse ablation (black line), with a smooth surface and no visible redeposition of the ablated material surrounding the crater. For BiBurst mode conditions shown by the blue and green profiles, the ablated depths are clearly deeper with similar crater profiles, indicating a larger ablated volume despite the smaller diameter of the craters. Ablated material redeposition surrounding the crater is obvious for the larger number of bursts ($N = 5$, $P = 25$), as also observed in figure 3.

For a more detailed investigation on the tendencies of the dimensions of the ablated spots, figures 5(a)–(c) show the dependence of depth on packet energy at various intrapulse

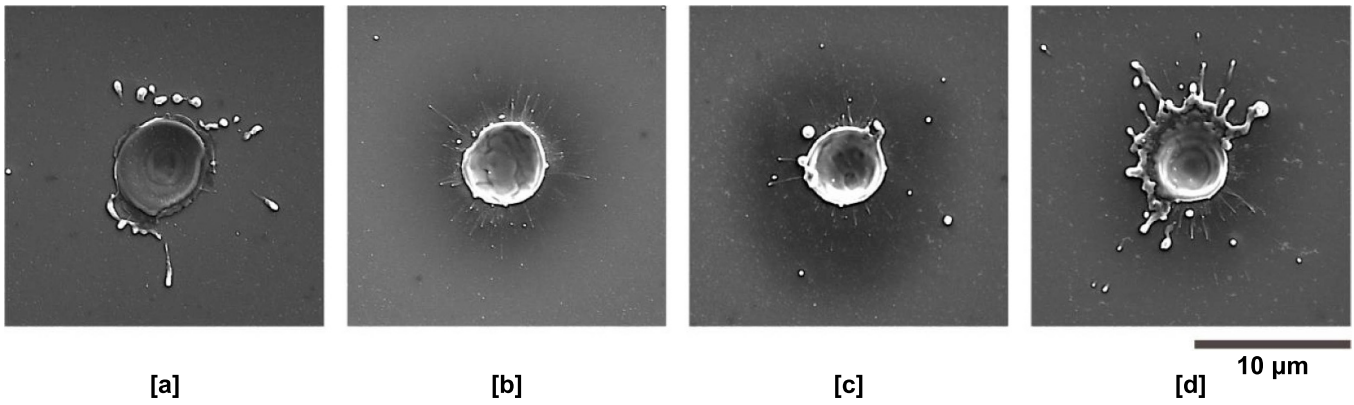

Figure 3. SEM images of the spots on the silicon surface ablated by delivering the same total energy of 0.53 μJ but with different burst mode configurations: (a) $N = 1$ $P = 1$ (1 pulse), (b) $N = 1$ $P = 25$ (one burst with 25 pulses), (c) $N = 2$ $P = 25$ (two bursts with 25 pulses per burst), and (d) $N = 5$ $P = 25$ (five bursts with 25 pulses per burst).

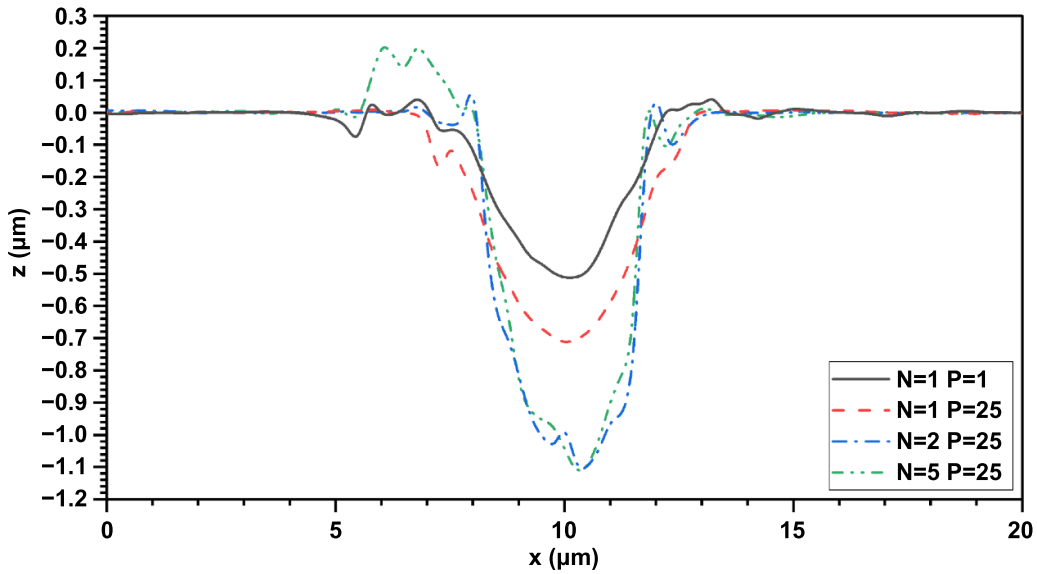

Figure 4. Profiles obtained by LSM for the cross sections of the ablated craters shown in figure 3.

numbers ($P = 1$, 2, 10, 20, and 25) for the MHz burst numbers N of 1, 2, and 5, respectively. As can be seen, almost all conditions of GHz burst mode (figure 5(a)), except $P = 2$, ablated deeper craters than the ones obtained by single pulse ablation at the same packet energy. This increase in ablated depth is even more noticeable for BiBurst conditions (figures 5(b) and (c)), and a 3.5 times deeper crater was ablated at 1 μJ for $N = 2$ and $P = 25$ as compared with the single pulse. Additionally, it can be seen that ablated depth for the single pulse ablation tends to saturate at higher energies, therefore, not being able to create deeper craters. In contrast, the use of burst mode and particularly BiBurst mode can ablate deeper craters by increasing the energy in the same range.

The presented results for depth measurements clearly show that GHz burst mode, and in particular BiBurst mode ablation, are more beneficial for creating deeper holes at the same total energy. In this case, multiple intrapulses with the same energy distribution can collaboratively contribute to ablate a deeper profile of the crater at the same spot. Additionally, the ultrafast succession of the pulses ensure that the entire process happens before the accumulated heat has enough time to expand to the surrounding material volume.

In contrast, when the energy is concentrated in one pulse (single pulse mode), the extremely intense and ultrashort single pulse peak cannot be absorbed efficiently because the contribution of electron heat conduction, which is important at high energy, regulates the degree of energy transfer within the target material [22].

The lateral dimensions of the ablated craters were also evaluated, as shown in figures 5(d)–(f). For GHz burst ablation (figure 5(d)), larger areas were ablated at the same delivered energy, especially for the series of $P = 20$ and $P = 25$ pulses per burst as compared with the single pulse irradiation. We speculate that latter pulses in GHz burst mode can be efficiently absorbed by transient incubation induced by preceding pulses due to the ultrashort time interval between each pulse even at the outer part of laser spot with smaller intensity, resulting in a larger ablation area. However, for BiBurst mode

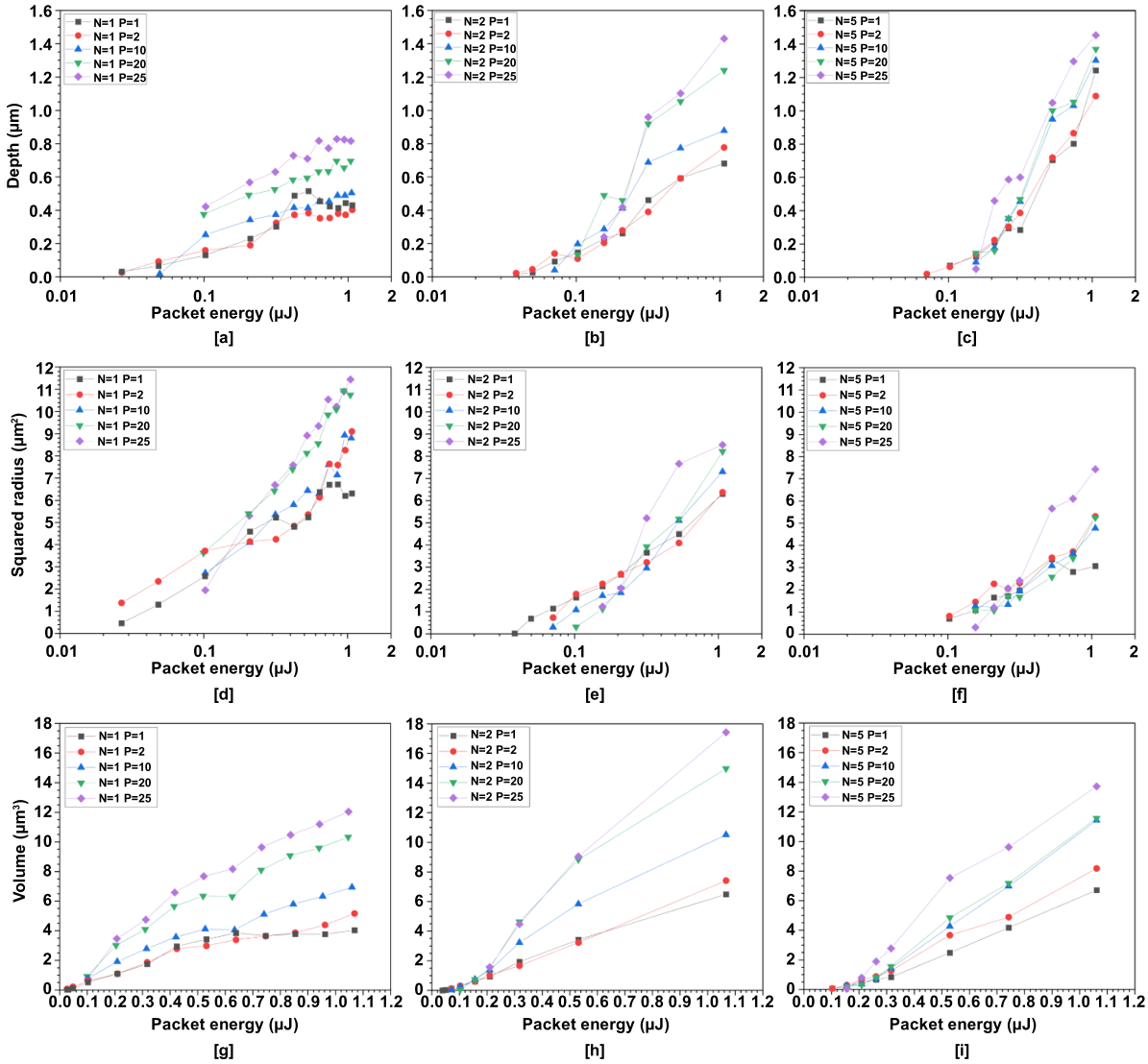

Figure 5. Dimensions ((a)–(c) depth, (d)–(f) squared radius, and (g)–(i) volume) of the ablated craters measured by LSM as a function of the packet energy delivered for the different burst mode configurations for intrapulse number P of 1, 2, 10, 20, and 25: (a), (d), (g) single burst mode ($N = 1$), BiBurst modes (b), (e), (h) with $N = 2$ and (c), (f), (i) with $N = 5$. The relative error for the depth measurements of the ablated craters has an average value of 5%.

conditions (figures 5(e) and (f)), similar or slightly smaller craters were produced at higher packet energies, because of the significantly reduced peak fluence and relatively longer interval between each burst. Specifically, since the peak fluence of each pulse in the bursts is $1/(N \times P)$ of that of the single pulse mode, the resulting ablated area becomes smaller due to the threshold effect when using a Gaussian beam [23]. Furthermore, transient incubation may relax before the next bursts arrive. This contrasts with the previously shown results for ablated depth, where BiBurst mode conditions resulted in distinctly deeper craters.

These diverging trends for ablated depth and ablated area can be also be understood from results previously obtained on the excitation of air plasma induced by the reflected laser radiation during irradiation with multiple pulses [24]. The interaction of the generated air plasma with the silicon plasma was found to enhance the shockwave expansion during silicon ablation in the longitudinal direction, which corresponds to the direction perpendicular to the sample surface, i.e. the direction along the crater depth. The results showed anisotropic expansion dynamics in different directions, which could be related to the differences observed in the ablated depth and area for burst mode ablation.

A good assessment of the detected competing tendencies between depth and area can be observed in the ablated volume, which is also measured by LSM and depicted in figures 5(g)–(i). When comparing the optimal conditions of the different ablation modes, it was observed that the ablated volume by BiBurst mode was 4.5 times larger than that of the single pulse for the same packet energy. This value was obtained as the ratio of 18 μm^3 of the ablated volume by BiBurst for $N = 2$ and $P = 25$ and 4 μm^3 by a single pulse ($N = 1$, $P = 1$) at the same packet energy of 1.1 μJ. To investigate this in more detail, the ablation efficiency was calculated from figures 5(g)–(i).

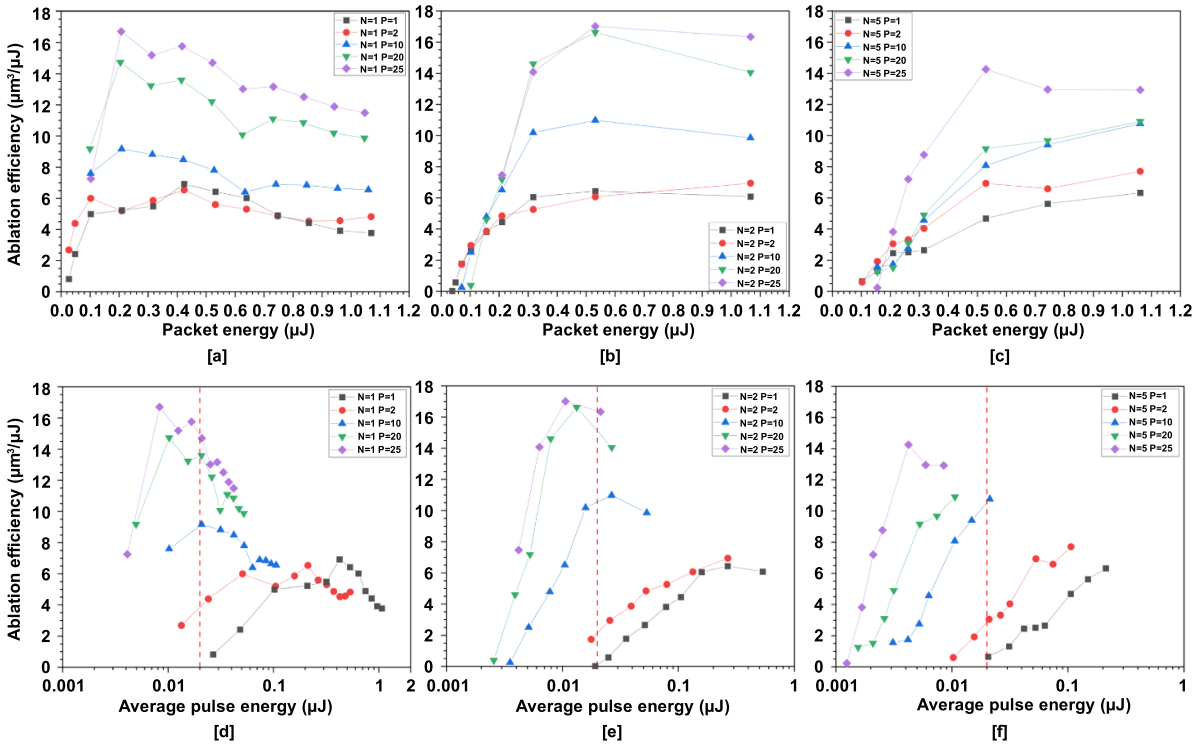

Figure 6. Ablation efficiency as a function of (a)–(c) the packet energy and (d)–(f) average pulse energy for the different burst mode configurations for intrapulse number P of 1, 2, 10, 20, and 25: (a), (d) single burst mode ($N = 1$), BiBurst modes (b), (e) with $N = 2$ and (c), (f) with $N = 5$.

Ablation efficiency is defined as the quotient of the ablated volume and the total energy (packet energy) delivered to produce the corresponding crater. The calculated efficiencies have been plotted against the packet energy for the different burst mode conditions in figures 6(a)–(c).

Ablation efficiency shows that GHz burst and BiBurst modes are more efficient in the ablation of silicon than the single pulse mode under almost all of the experimental conditions tested. Similar efficiencies were obtained by GHz burst and BiBurst modes, but BiBurst achieved the highest efficiencies above the critical energies, while GHz burst had the maximum efficiency at a relatively low energy around 0.2 μJ. This means that BiBurst is more effective for ablating larger volumes.

The highest ablation efficiencies were obtained with $P = 25$ for all configurations. GHz burst with 25 intrapulses corresponds to about 5 ns of the burst duration for the total processing time of a single burst. The highest ablation efficiencies obtained at the longest burst pulse are consistent with previous experiments carried out in similar experimental setups but with different configurations for the GHz burst mode [16, 17, 21].

As described above, the maximum ablation efficiency was obtained for energies in the low part of the explored packet energy range, close to the ablation threshold for GHz burst mode ablation (figure 6(a)). For BiBurst modes (figures 6(b) and (c)), the packet energy, where maximum efficiency is reached, shifted to higher energies, and the efficiency was almost saturated above these energies. These results indicate that in all cases relatively low average pulse fluences make the most efficient use of the absorbed incident laser radiation for material ablation. In particular, the optimum average pulse fluences for higher P may be below the ablation threshold of a single pulse. To confirm this, figures 6(a)–(c) were redrawn with average pulse energy on the horizontal axis in figures 6(d)–(f), respectively.

The spot size and ablation threshold energy were estimated from the series of ablated areas corresponding to the single pulse mode ($N = 1$, $P = 1$) in figure 5(d). Owing to the Gaussian spatial distribution of the laser pulses used, the ablation threshold energy E_{th} and the laser beam waist radius ω can be deducted from the logarithmic fit of the data according to equation (1) [25],

$$r^2 = \frac{\omega^2}{2} \ln\left(E/E_{\mathrm{th}}\right), \tag{1}$$

where E is the incident pulse energy. Results from the corresponding fit gave a laser beam waist of 1.9 μm in radius and an ablation threshold energy of 20 nJ, providing an ablation threshold fluence of 0.19 J cm^{-2}. The ablation threshold energy of 20 nJ, which is the minimum energy to induce ablation by a single pulse irradiation, is indicated by the red dashed lines in figures 6(d)–(f). As expected, the highest efficiencies in burst mode with P larger than 20 were achieved at average pulse energies lower than the ablation threshold for all configurations with a higher number of intrapulses, showing that the ablation threshold in burst mode conditions was

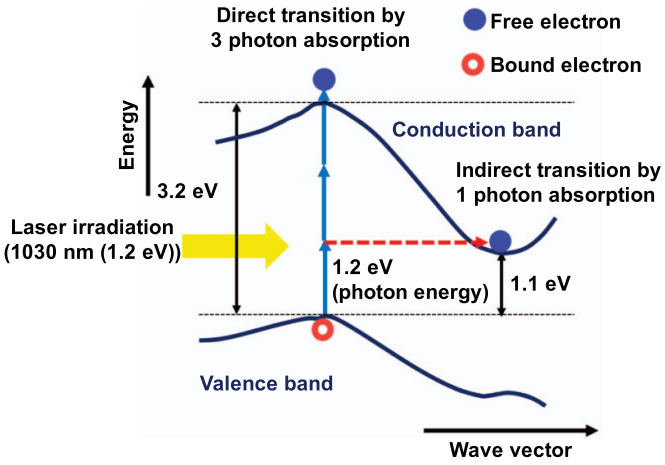

Figure 7. Schematic illustration of the Si band structure and electron excitation processes proposed as absorption mechanisms of the laser pulses.

distinctly reduced, similarly to what was observed in previous experiments [21].

The reduction of the threshold energy for burst mode conditions can explain the larger ablation area in GHz burst mode conditions. From equation (1), a lower threshold fluence leads to a larger spot where the fluence threshold is overcome, resulting in a larger area where ablation occurs [23]. However, smaller ablated areas were observed in BiBurst conditions. This indicates that the balance between the reduction of the threshold energy in burst mode and the lower energy carried by each of the pulses in the bursts determines the resulting surface area of the ablated crater.

In addition, an increased efficiency for ablation in burst mode can be understood through the absorption of the laser pulses and electron excitation processes in silicon, as shown in figure 7. In published research, it has been shown that at high intensities, usually reached by femtosecond laser pulses, absorption in silicon can take place through the direct band gap via multiphoton absorption [26]. For the case of the infrared wavelength used in our experiments, this requires the simultaneous absorption of three photons. In principle, single photon absorption is also possible across the indirect band gap at a stationary state. The probability of each absorption process depends on the laser intensity, and higher intensity, which is usual for single pulse mode, gives a higher probability of three photon absorption.

In contrast to that, the burst mode, with pulses possessing lower intensities, may preferentially induce single photon absorption and generate a larger number of free electrons as transient incubations. Once the free electrons are generated, they can efficiently absorb the laser energy by single photon absorption. Therefore, a larger number of free electrons can more efficiently deposit the laser energy in the material, achieving higher ablation efficiency. Specifically, the mechanism involves the absorption of the subsequent pulses in the burst by absorption sites (transient incubations) generated by preceding pulses in the same burst. These transient incubations correspond to the free electrons generated by interband excitation. The lifetime of free electrons in silicon is longer than several tens of ns [27], which is long enough to be absorbed by pulses in the latter part of the burst even with $P = 25$.

Another possible mechanism for enhanced ablation efficiency can be found in a recent publication, which demonstrated that the superficial melting of silicon can occur during irradiation by a single femtosecond laser pulse at fluences below the ablation threshold [28]. Furthermore, the metallic transition of melted silicon has been shown to contribute to a significant increase in the ablation rate of silicon during multiple pulse irradiation with consecutive pulses separated by delays comparable to the time separation between intraburst pulses presented in this paper [29].

These results can explain that in burst mode, instead of a predominant multiphoton absorption by three photons for single pulse mode, more efficient absorption is possible by the free carriers generated in silicon during burst mode irradiation. These free carriers are created during the non-thermal melting of silicon generated by the first pulse in the burst, even if the pulse energy is lower than the ablation threshold for single pulse ablation. After that, successive laser pulses in the burst can be absorbed via single photon absorption by promoting more electrons through the defects generated during non-thermal melting. The promoted electrons become free carriers in the conduction band that can absorb more photons from the following laser pulses in the burst, resulting in a higher absorption efficiency. In addition, the short duration of the process from the ultrafast pulse bursts contributes to absorption occurring before the generated free carriers recombine. This process more efficiently occurs at the laser fluence slightly below the ablation threshold fluence by single pulse irradiation. Therefore, BiBurst achieved the highest efficiencies at higher energies, while GHz burst had the maximum efficiency at a relatively low energy. Consequently, BiBurst is more effective for ablating larger volumes with high efficiency. Importantly, the short time duration of the process entails a reduction of detrimental thermal accumulation effects, increasing the efficiency of the ablation process in the GHz burst and the BiBurst modes compared to single pulse ablation.

The improved ablation efficiency for silicon strongly contrasts with opposite tendencies observed for the GHz burst and BiBurst mode ablation of metals. A major difference between semiconductors and metals is the absorption process. For semiconductors, absorption typically first takes place when bound electrons in the balance band are excited to the conduction band. Free electrons always induce absorption by metals, suggesting that the efficiency improvement for silicon in burst mode is associated with the absorption process and is likely due to an enhanced generation of free carriers at absorption sites originated by preceding pulses, as discussed above. Additionally, for metals, strong plasma shielding occurring during the burst irradiation is detrimental in multiple experimental conditions. Although in some cases it may be interesting for certain applications of the laser ablation process [18, 19, 30]. A feasible explanation for the presence of strong plasma shielding in metals and the apparent absence in semiconductor or dielectric materials can be obtained from laser-induced plasma

and shockwave expansion characterization experiments upon irradiation by multiple pulses [31]. However, available data only cover repetition rates far slower than the ultrafast regime reached in the GHz burst mode. For that, further experiments on laser-induced plasma and shockwave expansion visualization and analysis will be necessary for a deeper understanding of the laser-matter interaction processes happening during GHz burst and BiBurst mode laser ablation.

4. Conclusion

BiBurst (GHz bursts in MHz burst) mode laser ablation was investigated as a method to improve laser ablation performance while maintaining the benefits of ultrashort laser pulses, namely reducing the effect of heat in the area surrounding the processed spots, which offers good precision in the microfabrication of materials while achieving better ablation efficiencies for a higher throughput for practical use.

Specifically, it was observed that the distribution of the same laser power in multiple pulses at ultrafast repetition rates in bursts improves ablation efficiency compared to delivering the same power in a single pulse. For the optimal conditions, the volume ablated by BiBurst mode can be 4.5 times larger than that ablated by the single laser pulse with the same total energy delivered. Furthermore, the BiBurst mode achieved the highest ablation efficiency at higher packet energy as compared with the GHz, allowing a single packet to drill deeper with larger volume.

As a consequence, BiBurst mode laser ablation has been demonstrated as a suitable microfabrication technique for achieving higher throughput together with high quality processing in silicon. The obtained results provide a path for processing other materials that might show a similar laser-matter interaction behavior.

Acknowledgments

The authors would like to thank the Materials Characterization Support Unit, RIKEN CEMS for providing access to the SEM. This work was partially supported by MEXT Quantum Leap Flagship Program (MEXT Q-LEAP) Grant Number JPMXS0118067246.

ORCID iDs

Francesc Caballero-Lucas https://orcid.org/0000-0003-0335-9468
Koji Sugioka https://orcid.org/0000-0002-7174-5961

References

[1] Vorobyev A Y and Guo C L 2013 Direct femtosecond laser surface nano/microstructuring and its applications *Laser Photonics Rev.* **7** 385–407
[2] Malinauskas M, Žukauskas A, Hasegawa S, Hayasaki Y, Mizeikis V, Buividas R and Juodkazis S 2016 Ultrafast laser processing of materials: from science to industry *Light Sci. Appl.* **5** e16133
[3] Sugioka K 2017 Progress in ultrafast laser processing and future prospects *Nanophotonics* **6** 393–413
[4] Sugioka K and Cheng Y 2014 Ultrafast lasers—reliable tools for advanced materials processing *Light Sci. Appl.* **3** e149
[5] Li R *et al* 2020 Stimuli-responsive actuator fabricated by dynamic asymmetric femtosecond Bessel beam for *in situ* particle and cell manipulation *ACS Nano* **14** 5233–42
[6] Zhu S W *et al* 2020 High performance bubble manipulation on ferrofluid-infused laser-ablated microstructured surfaces *Nano Lett.* **20** 5513–21
[7] Hu Y L *et al* 2020 Chiral assemblies of laser-printed micropillars directed by asymmetrical capillary force *Adv. Mater.* **32** 2002356
[8] Liu X, Du D and Mourou G 1997 Laser ablation and micromachining with ultrashort laser pulses *IEEE J. Quantum Electron.* **33** 1706–16
[9] Momma C, Nolte S, Chichkov B N, Alvensleben F V and Tünnermann A 1997 Precise laser ablation with ultrashort pulses *Appl. Surf. Sci.* **109–10** 15–19
[10] Ancona A, Röser F, Rademaker K, Limpert J, Nolte S and Tünnermann A 2008 High speed laser drilling of metals using a high repetition rate, high average power ultrafast fiber CPA system *Opt. Express* **16** 8958–68
[11] Kato J I, Takeyasu N, Adachi Y, Sun H B and Kawata S 2005 Multiple-spot parallel processing for laser micronanofabrication *Appl. Phys. Lett.* **86** 044102
[12] Obata K, Koch J, Hinze U and Chichkov B N 2010 Multi-focus two-photon polymerization technique based on individually controlled phase modulation *Opt. Express* **18** 17193–200
[13] Li Y and Hong M 2020 Parallel laser micro/nano-processing for functional device fabrication *Laser Photonics Rev.* **14** 1900062
[14] Eaton S M, Zhang H B, Herman P R, Yoshino F, Shah L, Bovatsek J and Arai A Y 2005 Heat accumulation effects in femtosecond laser-written waveguides with variable repetition rate *Opt. Express* **13** 4708–16
[15] Kerse C *et al* 2016 Ablation-cooled material removal with ultrafast bursts of pulses *Nature* **537** 84–88
[16] Bonamis G, Audouard E, Hönninger C, Lopez J, Mishchik K, Mottay E and Manek-Hönninger I 2020 Systematic study of laser ablation with GHz bursts of femtosecond pulses *Opt. Express* **28** 27702–14
[17] Hodgson N, Allegre H, Starodoumov A and Bettencourt S 2020 Femtosecond laser ablation in burst mode as a function of pulse fluence and intra-burst repetition rate *J. Laser Micro Nanoeng.* **15** 236–44
[18] Žemaitis A, Gaidys M, Gečys P, Barkauskas M and Gedvilas M 2021 Femtosecond laser ablation by bibursts in the MHz and GHz pulse repetition rates *Opt. Express* **29** 7641–53
[19] Metzner D, Lickschat P and Weißmantel S 2021 Optimization of the ablation process using ultrashort pulsed laser radiation in different burst modes *J. Laser Appl.* **33** 012057
[20] Förster D J, Jäggi B, Michalowski A and Neuenschwander B 2021 Review on experimental and theoretical investigations of ultra-short pulsed laser ablation of metals with burst pulses *Materials* **14** 3331
[21] Mishchik K, Bonamis G, Qiao J, Lopez J, Audouard E, Mottay E, Hönninger C and Manek-Hönninger I 2019 High-efficiency femtosecond ablation of silicon with GHz repetition rate laser source *Opt. Lett.* **44** 2193–6
[22] Choi T Y and Grigoropoulos C P 2002 Plasma and ablation dynamics in ultrafast laser processing of crystalline silicon *J. Appl. Phys.* **92** 4918–25
[23] Garcia-Lechuga M, Utéza O, Sanner N and Grojo D 2020 Evidencing the nonlinearity independence of resolution in femtosecond laser ablation *Opt. Lett.* **45** 952–5

[24] Wang Q S, Jiang L, Sun J Y, Pan C J, Han W N, Wang G Y, Wang F F, Zhang K H, Li M and Lu Y F 2018 Structure-mediated excitation of air plasma and silicon plasma expansion in femtosecond laser pulses ablation *Research* **2018** 5709748

[25] Liu J M 1982 Simple technique for measurements of pulsed Gaussian-beam spot sizes *Opt. Lett.* **7** 196–8

[26] Schultze M *et al* 2014 Attosecond band-gap dynamics in silicon *Science* **346** 1348–52

[27] de Laurentis M and Irace A 2014 Optical measurement techniques of recombination lifetime based on the free carriers absorption effect *J. Solid State Phys.* **2014** 291469

[28] Florian C *et al* 2021 Single femtosecond laser-pulse-induced superficial amorphization and re-crystallization of silicon *Materials* **14** 1651

[29] Zhao X and Shin Y C 2014 Ablation enhancement of silicon by ultrashort double-pulse laser ablation *Appl. Phys. Lett.* **105** 111907

[30] Obata K, Caballero-Lucas F and Sugioka K 2021 Material processing at GHz burst mode by femtosecond laser ablation *J. Laser Micro/Nanoeng.* **16** 19–23

[31] Guo B S, Sun J Y, Lu Y F and Jiang L 2019 Ultrafast dynamics observation during femtosecond laser-material interaction *Int. J. Extreme Manuf.* **1** 032004